ANNALS OF GEOPHYSICS, 68, 6, NS692, 2025; doi:10.4401/ag-9298
OPEN ACCESS

Geophysical prospection for sustainable groundwater management: strategies for regional water resource optimization

Allex Raiol Cardoso Medeiros[1], Franklim Roberto Lima dos Santos[1], Willianny Carolina Castellanos Veracierta[1], Herson Rocha[*,2], João Andrade dos Reis Júnior[3]

(1) GeoProspecto Solutions in Geophysics Company Inc. (GEOPROSPECTO), Pará, Brazil
(2) Federal University of Rio de Janeiro (UFRJ), Polytechnical Institute (IPOLI), Rio de Janeiro, Brazil
(3) Federal Rural University of Amazônia (UFRA), Campus Capanema, Pará, Brazil

Article history: received February 20, 2025; accepted December 3, 2025

Abstract

This study employs an integrated geophysical approach, combining Electrical Resistivity Tomography (ERT) with Dipole-Dipole, Pole-Dipole, and Pole-Pole arrays and Vertical Electrical Sounding (VES) with a Schlumberger array, to delineate groundwater resources in the municipality of Sucupira do Norte, Maranhão, Brazil, a region with water scarcity. The survey successfully identified three aquifer units: a shallow unconfined aquifer (<35 m depth; 10 to 100 Ω·m) considered unsuitable for use due to the risk of contamination, and two deeper confined aquifers. Aquifer B was identified at depths of 60 to 90 m, with resistivity values of 500 to 600 Ω·m, while the main target, Aquifer C, was found at depths of 140 to 190 m, with lower resistivity values of 50 to 100 Ω·m, indicative of water-saturated sandstones within the Pedra de Fogo Formation. Based on these results, two specific drilling locations were defined, with recommended depths of 160 m and 270 m to ensure sustainable production. The results demonstrate the effectiveness of integrating Electrical Resistivity Tomography (ERT) and Vertical Electrical Sounding (VES) to reduce uncertainty in exploration and provide a robust strategy for the sustainable management of groundwater in drought-prone regions.

Keywords: Aquifers; Electrical Resistivity; Groundwater Exploration; Hydrogeology; Well Drilling

1. Introduction

One of the main causes of changes in the hydrological regime of Amazonian rivers is the combination of deforestation and wildfires, which intensifies climate change. In recent years, there has been an increase in these factors, resulting in more frequent and severe droughts and floods, with less time between these extreme events. In the Amazon and northeastern Brazil, the increase in tidal amplitude (ebb and flow) has reached up to 1.6 m, causing rivers to dry up earlier than expected or, conversely, flood unexpectedly. This shift has a significant impact, particularly in flooded forest areas, affecting economic activities such as navigation and the livelihoods of riverine

populations who depend on agriculture and fishing (Aguiar et al., 2024; Bastos et al., 2019; Rossi et al., 2024; Zanin et al., 2024).

Beyond biological interactions, the flood regime, with its predictability and regularity, governs biogeochemical cycles, geomorphological processes, and the expansion of biota adapted to these conditions. Floodplain areas have been severely impacted by the increased frequency of droughts and floods, with the flood duration increasing by over 50 days annually in 23% of the lowland Amazon floodplains in recent years (Zanin et al., 2024).

Meanwhile, a contrasting pattern has emerged, with increased rainfall in the northern Amazon and reduced rainfall in the southern region. This discrepancy is likely due to increased deforestation, wildfires, and large infrastructure projects, such as hydropower plants, in southern Amazonia. In contrast, better-preserved areas are found in the northern region. Reduced rainfall, combined with rising temperatures in deforested areas, has led to decreased evapotranspiration, contributing to a lower-than-expected rainfall scenario in much of the region (Rossi et al., 2024).

Given this situation, it is essential to finance initiatives aimed at alleviating the suffering of local populations. The drought has isolated thousands of people, cutting off their access to food, medicine, and, most importantly, drinking water. Key actions include installing rainwater cisterns, drilling deeper wells to reach the water table or confined aquifers, and distributing emergency water treatment kits.

The Amazon region has vast underground water reserves in the form of aquifers. However, studying these aquifers is challenging due to their complexity, with layers varying in depth from 20 m to over 250 m and diverse geological formations. In the Northeast, the irregular and cyclic nature of rainfall, marked by periodic droughts, demands an integrated management approach for surface and groundwater resources (Correia Filho et al., 2011; Bastos et al., 2019). However, the lack of regionwide studies hampers the effective management of these resources, reducing the potential for sustainable use.

Mendes et al. (2014) integrated geophysical well log data with six vertical electrical soundings (VES) to develop a geoelectrical model of the subsurface. Their results delineated two principal layers: a shallow, more resistive unit less than 30 meters thick, interpreted as the sandy and hydrogeologically weak Itapecuru Formation, underlain by a low resistivity substrate correlated to the shale dominated Codó Formation. The study concluded that the aquifer potential resides not in the shallow sands but within the deeper Codó Formation's interbedded sandstone and shale sequences, identifying it as the most promising solution for the city's water supply.

Rocha et al. (2019) conducted a hydrogeophysical investigation to support the development of a water supply system at Nova Vida Farm in Parauapebas, southeastern Pará, Brazil. The farm, which cultivates crops such as corn, beans, and soybeans and raises beef cattle for export, faced water scarcity during the dry season due to its reliance on shallow artesian wells and storage cisterns. To address this, the study employed vertical electrical sounding (VES) and electromagnetic profiling using a horizontal loop electromagnetic (HLEM) system across eight frequencies (ranging from 110 to 14,080 Hz). The results, visualized through VES graphs and electromagnetic isocontour maps, identified optimal locations for new well installations, offering a sustainable solution for the farm's water management challenges.

Moreover, decisions regarding drought management actions require a thorough understanding of the location, characterization, and availability of water sources (Veras et al., 2019). Before drilling wells for supply, especially in urban areas, it is crucial to assess the vulnerability of aquifers to contamination by heavy metals and their capacity to provide potable water during prolonged droughts. Groundwater must be used sustainably, recognizing it as a vital natural, ecological, social, and economic resource, especially in the Northeast, where it is a critical tool in combating drought and promoting public health by reducing waterborne diseases.

While geoelectrical methods are well-established in groundwater exploration, this study's novelty lies in its integrated multimethod approach tailored to address acute water scarcity in a critically understudied region. We combine Electrical Resistivity Tomography (ERT) through Electrical Traversing (employing Dipole Dipole, Pole Dipole, and Pole Pole arrays) with Vertical Electrical Sounding (VES-Schlumberger) to synergistically maximize both lateral and vertical resolution of the subsurface. This strategy is deployed in the Amazon-Semiarid transition zone of Maranhão, Brazil, a region severely impacted by climate variability and lacking detailed hydrogeological studies.

The primary contribution of this work is to generate a robust, low-cost hydrogeological model that accurately identifies deep confined aquifers within the complex geological framework of the Parnaíba Basin. By moving beyond regional reconnaissance to provide specific, actionable drilling targets for tubular wells, this research delivers a practical and strategic tool for sustainable water resource management, directly mitigating the effects of prolonged drought for vulnerable communities and livestock.

2. Physiographic aspects and geological context

The town of Sucupira do Norte is located in the Eastern Maranhão mesoregion, within the Chapada do Alto Itapecuru microregion, covering an area of 1,074.4 km^2. Its geographic coordinates are approximately 6°28′12″S and 44°11′24″W, according to the Silva et al. (2016). It is bordered by Colinas to the north, São Domingos do Azeitão to the south, Pastos Bons to the east, and Mirador and Paraibano to the west (Fig. 1).

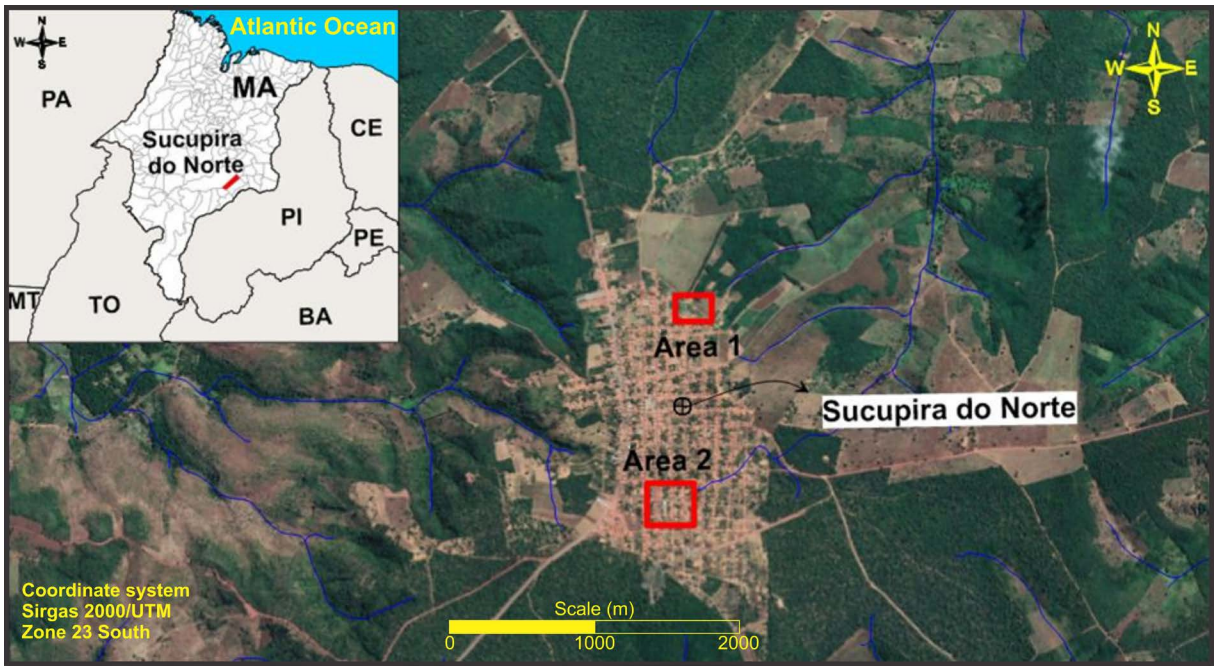

Figure 1. Location map of the study area in northeastern Brazil, highlighting the urban zone of Sucupira do Norte, Maranhão state. The abbreviations (MA, PA, MT, TO, BA, PI, CE, PE, BA) meaning the name of the states (Maranhão, Pará, Mato Grosso, Piauí, Ceará, Bahia) and the red polygons denote the areas where electrical resistivity tomography (ERT) and vertical electrical sounding (VES) surveys were conducted.

For our hydrogeological investigation using geophysical surveys, two study areas (Area 1 and Area 2) were selected within the urban zone of Sucupira do Norte. These sites are approximately 700 m apart, allowing for comparative analysis of groundwater conditions in different parts of the municipality. Area 1 is situated at coordinates 6°28′23.24″S and 44°11′17.94″W, while Area 2 is located at 6°29′7.18″S and 44°11′23.16″W.

The state of Maranhão, located in a transitional zone between the semiarid climate of the Northeastern interior and the humid equatorial climate of the Amazon, experiences significant climatic and rainfall variations due to its north-south extension. The western region is dominated by a hot and humid tropical climate typical of the Amazon, while the rest of the state is characterized by a hot and semi-humid tropical climate (Dos Reis et al., 2020).

Temperatures across Maranhão are generally high, with annual averages exceeding 24°C, reaching 26°C in the north. The rainfall regime features two well-defined seasons. The rainy season, from December to May, records state averages of 290.4 mm, peaking in March. Conversely, the dry season, from June to November, averages just 17.1 mm, with the lowest rainfall in August. The western region, dominated by a hot and humid tropical climate, experiences heavy rainfall nearly year-round, exceeding 2,000 mm. In other regions, where the semi-humid tropical climate prevails, precipitation reaches 1,250 mm, dropping to 1,000 mm in the southeast (Dos Reis et al., 2020).

Maranhão's territory is a large platform sloping towards the Atlantic Ocean, with relief characterized by features typical of sedimentary basins, shaped by prolonged erosion cycles. The highest altitudes are in the southern part, in the Chapada das Mangabeiras, bordering Tocantins, while the lowest are near the northern coast (Barreto et al., 2024).

Ab'Saber (1960) classified the state's relief into two major units: plains, occupying 60% of the territory, including coastal, fluvio-marine, and sublittoral plains; and plateaus, covering 40%, with elevations above 200 m. Barreto et al.

(2024) identified various relief forms, such as high and low plateaus, undulating surfaces, the Baixada Maranhense, terraces and floodplains, coastal plateaus, sandbanks, dunes, the Maranhense Gulf, and the Coastal Lowlands.

In eastern Maranhão, plateaus interspersed with hills and mountains dominate. Drainage follows zones of weakness in sedimentary rocks, shaping flat and sloping landscapes, alongside residual flat-topped hills. The Itapecuru Dissected Plateau, with altitudes between 140 and 200 m, features hills and ridges with pedimented valleys. Residual hills and plains are also present, with the area intersected by the Itapecuru River displaying flat relief, corresponding to an ancient terrace level. The Tabuleiros do Médio Itapecuru area is marked by dissected tops in ridges and hills, with altitudes between 180 and 240 m. The Tabuleiros do Parnaíba, on the left bank of the river, exhibit irregular relief, ranging from 20 to 400 m, with dissected hills and mountains (Barreto et al., 2019). The Sublittoral Plateaus have flat relief, cut by south-north drainage, with gentle hills and ridges along the drainage (Klein and Short, 2023).

The variations in climate, relief, and soil across Maranhão contribute to a diverse range of natural environments. The state's vegetation reflects the transitional climate conditions between the Amazon and the semiarid Northeast. In the Itapecuru Dissected Plateau, the original forest vegetation has been largely replaced by agricultural and subsistence farming activities. The regional climate ranges from subhumid to semiarid, with annual precipitation between 1,400 and 1,600 mm (Silva-Moraes et al., 2019).

In the Plateau de Caxias area, vegetation is marked by the transition between savanna and forest, with the former predominating. The climate is subhumid to semiarid, with annual precipitation between 1,300 and 1,500 mm. In the Tabuleiros do Médio Itapecuru area, the vegetation is also characterized by the interaction between savanna and forest, with parts replaced by agricultural activities. The climate ranges from subhumid to semiarid, with precipitation between 1,200 and 1,400 mm (Pereira et al., 2022). In the Tabuleiros do Parnaíba, savanna and forest interact, with open tree savanna predominating. Some areas have been altered for agriculture and subsistence farming, and the regional climate is subhumid to semiarid, with annual precipitation between 1,100 and 1,400 mm (Feitosa et al., 2024).

The region's soils include Yellow Latosol, Dark Red Latosol, and Litholic Soils. Yellow Latosol is a deep, well-drained soil with yellowish horizons and medium to clayey texture. Predominantly dystrophic, it can also be acid, with high aluminum saturation and low nutrient levels. It is found in the tops of plateaus, which may be low and dissected or high and extensive, with flat relief and slight undulations. The most common parent material consists of sandy-clay and clay covers derived from or superimposed on sedimentary formations (Dantas et al., 2014).

According to Brito Neves (1998), the municipality of Sucupira do Norte lies within the domains of the Parnaíba Sedimentary Basin, which was formed over Cambro-Ordovician rifts such as Jaibaras, Jaguarapi, Cococi/Rio Jucá, São Julião, and São Raimundo Nonato. This basin includes the Silurian (Serra Grande Group), Devonian (Canindé Group), and Carboniferous-Triassic (Balsas Group) supersequences as described by Góes and Feijó (1994) (Fig. 2).

In the municipality of Sucupira do Norte, the Mearim Group is represented by the Pastos Bons (PSB) and Corda (COR) Formations from the Jurassic period, as well as the Sardinha (SAR) Formation from the Cretaceous period. The Pastos Bons Formation consists of greenish and reddish-brown shales and sandstones that occur near the homonymous town in Maranhão (Brito and Gallo, 2002; Vaz et al., 2007).

The Pedra de Fogo Formation (PEF) is a Permian age stratigraphic unit within the Parnaíba Basin of northeastern Brazil, forming part of the Balsas Group. Composed primarily of sandstones, siltstones, and shales with interbedded limestones and evaporites (including gypsum and anhydrite), this formation was deposited in shallow marine to coastal environments, likely lagoonal or estuarine settings influenced by cyclical sea-level fluctuations. The unit is particularly notable for its well-preserved fossil assemblages, including fish, conchostracans, and plant remains, which provide valuable insights into Permian paleoecology. Beyond its paleontological significance, the Pedra de Fogo Formation has economic importance due to its phosphate deposits, which are valuable for fertilizer production, and have been investigated for potential unconventional gas resources such as shale gas (see Fig. A1 in the Appendix).

Hydrogeologically, it functions as a secondary aquifer in some areas, though its water-bearing potential is often limited by the low permeability of its shale-rich intervals. Regionally, the formation serves as a key stratigraphic marker for Permian deposits in Brazil and correlates with other Gondwanan basins, reflecting the arid to semiarid climatic conditions and marine influences that characterized western Gondwana during this period. Its depositional features and fossil content collectively offer important clues about the paleoenvironmental and tectonic evolution of the Parnaíba Basin during the Permian (Góes and Feijó, 1995; Vaz et al., 2007).

Lithologically, the Pastos Bons Formation can be divided into two sections. The lower section typically begins with a conglomerate, whose composition varies depending on the underlying strata. Above the conglomerates are found greenish to whitish cream-colored sandstones, clayey, with thin to medium subrounded grains, and slightly glossy. Locally, limestone intercalations occur, some of which are silicified. The upper section is more sandstone

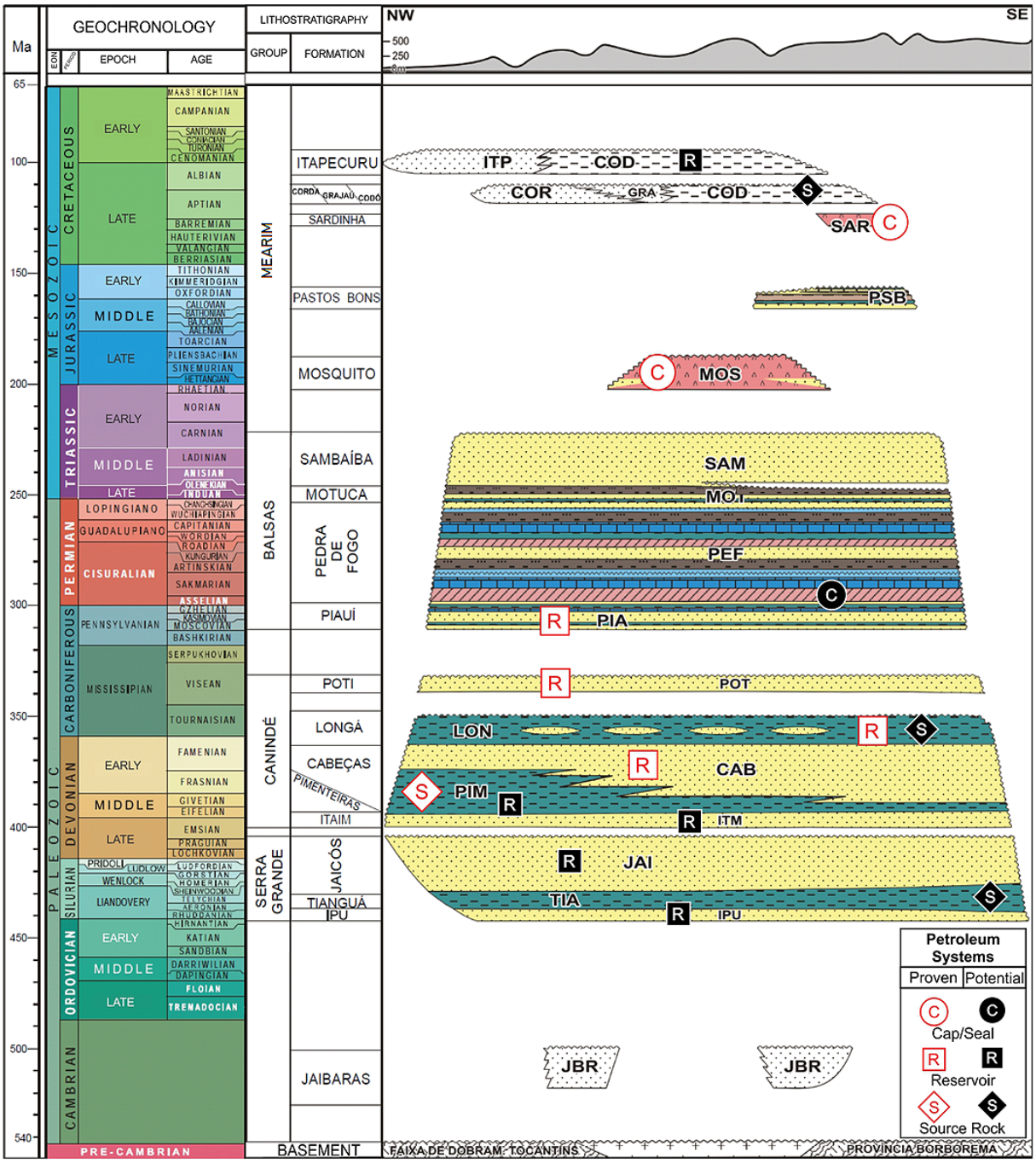

Figure 2. Stratigraphic chart of the Parnaíba Basin, showing the characteristics of the depositional mega sequences that compose the sedimentary fill of the basin (modified from Vaz et al., 2007).

rich and consists primarily of pinkish to reddish sandstones, sometimes whitish, thin to silty, and clayey, with intercalations of pinkish to gray greenish shales and siltstones, some of which are fossiliferous. Planar parallel crossbedding is the predominant structure in the sequence. This formation has the greatest geographical expression in the region, cropping out to the west and extending southwest of Sucupira do Norte (Correa-Martins, 2019).

According to Oliveira et al. (2018), the Corda Formation (COR) is a section of sediments about 80 m thick, with Jurassic aged siliceous intercalations, resting on basalts of the Mosquito Formation and unconformably overlain by the basalts of the Sardinha Formation (SAR). When the Corda Formation is in contact with the Mosquito basalts, its lithological sequence begins with coarse to conglomerate sandstones, reddish-brown to purplish. When this unit lies directly on other formations in the absence of the Mosquito basalts, the lithological sequence consists mainly of clayey, reddish-brown sandstones with largescale crossbedding.

Locally, these sandstones are highly calciferous, as observed in Imperatriz and Grajaú, in Maranhão, and Tocantinópolis, in Tocantins. In the middle section of the Corda Formation, intercalations of claystone, silty claystone, and shale layers with crossbedding may occur. The top of the unit contains purplish and reddish-brown medium to coarse sandstones with rounded and dull grains, containing quartz pebbles and largescale planarparallel stratification. The thickness of the Corda Formation ranges from 30 m in the Imperatriz region to 84 m near Pastos Bons. In the Fortaleza dos Nogueiras region, its thickness is around 80 m, with widespread outcrops in nearly all quadrants of Sucupira do Norte, especially in the municipal seat (De Castro et al., 2018; Da Silva et al., 2020).

The Sardinha Formation (SAR) is characterized by basalts cropping out near the Sardinha village, southwest of Barra do Corda. These basalts are positioned above the Corda Formation (COR) and below the Itapecuru Formation (ITP), with a typical thickness ranging from 100 to 300 meters (locally up to 350 m in depocenters). Photointerpretation studies showed that the Sardinha Formation is topographically at the same level or slightly higher than the Grajaú Formation (GRA) sandstones, reflecting its variable depositional architecture (Reimold et al., 2022). Thickness variations are attributed to fluvial deltaic channel stacking and basin subsidence, with the thickest sequences occurring in the central to northern parts of the basin (Vaz et al., 2007; Góes and Feijó, 1994). However, field observations led these authors to conclude that these units are stratigraphically below the Grajaú sandstones, as they are unconformable over the Corda Formation and interdigitated with the Codó Formation (COD). The Codó Formation consists of organic rich mudstones, carbonates, gypsum, anhydrite, and subordinate sandstones, deposited in a lacustrine environment influenced by marine incursions during the Late Aptian to Early Albian (Rodrigues, 1995; Mendes, 2007). Like the Mosquito Formation, the lava flows of the Sardinha Formation erupted through fissures in subaerial and continental conditions.

3. Hydrogeological domains and correlation with water supply wells

Groundwater is defined as the water located in the saturated zone, where all porous spaces are filled with water. Geological units capable of storing and transmitting significant amounts of water are called aquifers (Castany, 1982; Hiscock et al., 2014).

Groundwater systems are generally categorized into three main geological domains (Schwartz and Zhang, 2024): (i) igneous and metamorphic rocks, which store water through secondary porosity resulting from fractures, forming what is known as “fractured aquifers” (Costa, 2000); (ii) carbonate rocks, such as limestone and dolomite, where water storage occurs through secondary porosity developed by mineral dissolution and leaching, characterizing “karst aquifers”; and (iii) consolidated and unconsolidated sediments, including sandstones, alluvial deposits, and eolian dunes, which typically form porous or intergranular aquifers due to primary porosity between grains.

The hydrogeology of the municipality of Sucupira do Norte encompasses two distinct domains: (i) a fractured aquifer associated with basalts and/or diabases from the Sardinha Formation; and (ii) a porous or intergranular aquifer related to the consolidated sediments of the Pastos Bons and Corda Formations. The Pastos Bons Formation, characterized by very thin-grained siltstones, shales, and clayey sandstones, predominantly pelitic lithologies, functions as an aquitard with low potential for groundwater storage and flow. This unit is typically exploited in the region through shallow tubular wells and hand-dug wells, commonly known as “Amazonian wells”. Tubular wells and hand-dug wells are two methods used to access groundwater, but they differ in both construction and depth. Tubular wells are typically narrow and can reach greater depths by drilling or driving a pipe/casing into the ground. In contrast, hand-dug wells are much wider but significantly shallower, and they are constructed manually by digging into the ground.

On the other hand, the Corda Formation acts as an unconfined to confined aquifer, predominantly composed of thin to medium-grained quartz sandstones with intercalations of clayey horizons and occasional siltstone and shale layers. Due to its lithological composition, the Corda Formation exhibits moderate permeability (~50-200 mD), classifying it as an aquifer of medium potential, according to Freeze and Cherry (1979). Wells that tap into this aquifer typically range in depth from 150 m to 700 m, based on lithological profiles from wells drilled by the Brazilian Mineral Resources Research Company (CPRM) in the state of Maranhão. The average thickness of this formation is approximately 160 m.

Recharge occurs through direct precipitation infiltration in recharge areas, as well as upward vertical infiltration from underlying formations and surface water drainage during high-flown periods. Discharge zones include the surface drainage network, which receives groundwater during dry periods, as well as evapotranspiration and artificial extraction via drilled wells.

The Sardinha Formation, consisting of basaltic and/or diabase rocks, lacks significant primary porosity, so groundwater occurrence is controlled by secondary porosity, predominantly within fractures and fissures. Water flow is limited to open fractures, leading to the development of small-scale, discontinuous reservoirs typical of fractured aquifers (Correia Filho et al., 2011). Due to these hydrogeological constraints, the Sardinha Formation exhibits minimal aquifer potential, and excessive exploitation through tubular wells can quickly deplete the available reserves. The limited dimensional and hydraulic characteristics of this aquifer, combined with predicted recharge reductions during prolonged droughts and challenges in natural replenishment, make it a marginally exploited groundwater resource in the region.

Only two vertical tubular wells (Well A and Well B) were identified in the Groundwater Information System (SIAGAS) within the municipal headquarters. Well A has a flow rate of 6 m^3/h, with a static water level located between 168 m and 186 m depth. This well contains three filter screens: the first is 13 m long, positioned between 197 m and 210 m (Pastos Bons Formation); the second is 19 m long, located between 335 m and 354 m; and the third is 18 m long, spanning 372 m to 390 m. The diameters of borehole Well A are 219 mm between 0 and 130 m, 152 mm between 130 and 302.5 m, and 101 mm between 302.5 and 400 m.

In contrast, Well B exhibits a lower flow rate of 3 m^3/h, with its static water level situated between 252 m and 260 m depth, just above the brown calciferous shale. This well is equipped with a single screen, measuring 57 m in length, installed between 352 m and 409 m (Pedra de Fogo Formation). The diameters of borehole Well B are 374.65 mm between 0 and 101 m, 311.15 mm between 101 and 309 m, and 244.47 mm between 309 m and 445 m.

These observations indicate the presence of two distinct aquifer types in the region: granular (or porous) aquifers and fractured (or fissured) aquifers, each offering different hydrogeological potentials. Figure 3 and Table 1 illustrate the hydrogeological characteristics of the identified wells, providing detailed information on groundwater extraction conditions, lithological and geological descriptions of the subsurface layers, well depths, and the associated geological formations.

Table 1. Lithological and geological description of wells A and B.

Well	Depth (m)	Lithological Description	Hydrogeological Character	Geological Formation
A	0-26	Yellow-orange lateritic soil.	Porous (weathered layer)	Corda Formation
	26-100	Very thin sandstone, clayey siltstone, reddish-brown in color.	Porous aquifer	
	100-168	Black basalt.	Fractured aquifer	Sardinha Formation
	168-225	Thin brown sandstone with thin intercalations of gray siltstone, occasionally pyritic and carbonatic.	Aquitard	Pastos Bons Formation
	225-400	Thin sandstone in cream and brown tones with intercalations of thin beds of siltstone and carbonatic shale.	Porous aquifer	Pedra de Fogo Formation
B	0-12	Yellow-brown sandy soil, lateritized.	Porous (weathered layer)	Corda Formation
	12-100	Thin brown sandstone with intercalations of calciferous siltstone and silex.	Porous aquifer	
	100-180	Black diabase.	Fractured aquifer	Sardinha Formation
	180-260	Thin white-orange sandstone with intercalations of gray and brownish carbonatic shale.	Aquitard	Pastos Bons Formation
	260-270	Brown calciferous shale.	Aquitard	Pedra de Fogo Formation
	270-309	Very thin yellow-orange sandstone with intercalations of carbonatic siltstone.	Porous aquifer	
	309-440	Sandstone with thin to medium grains, yellow in color, intercalated with silexite layers.	Porous aquifer	

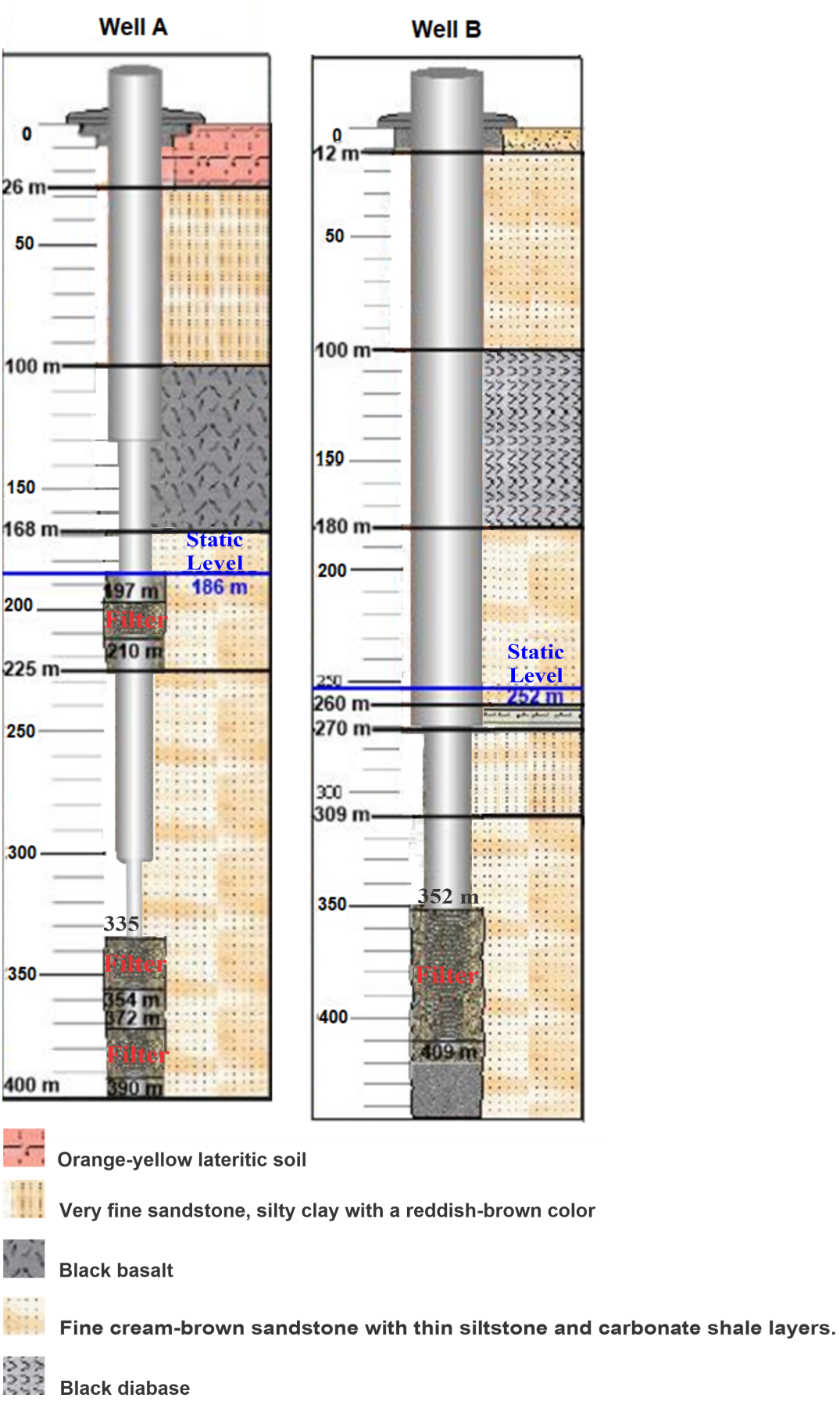

Figure 3. Comparison of the construction logs for Well A and Well B, showing lithological descriptions, geological formations, and the depth of filter screens.

4. Materials and Methods

4.1 Data acquisition

For the geophysical resistivity survey, the GeoElectric DC Series GD System, model GD10, manufactured by Geomative Company Inc, was used (Fig. 4). Stainless steel electrodes with a diameter of 12.5 mm and a length of 50 cm were employed (Fig. 5). Four spools of electrical cables were used to connect the electrodes to the equipment for measurement purposes. Data acquisition took place during the Brazilian summer of 2022, and data were collected in the time domain, with current injection intervals of 4 s at 5 A, and a constant injection of 1000 V, powered by an external source (a 7 kVA generator). The geographic locations and elevations of the VES points were obtained using a Garmin CSx GPS model.

Figure 4. GeoElectrical System equipment, model GD10, manufactured by Geomative.

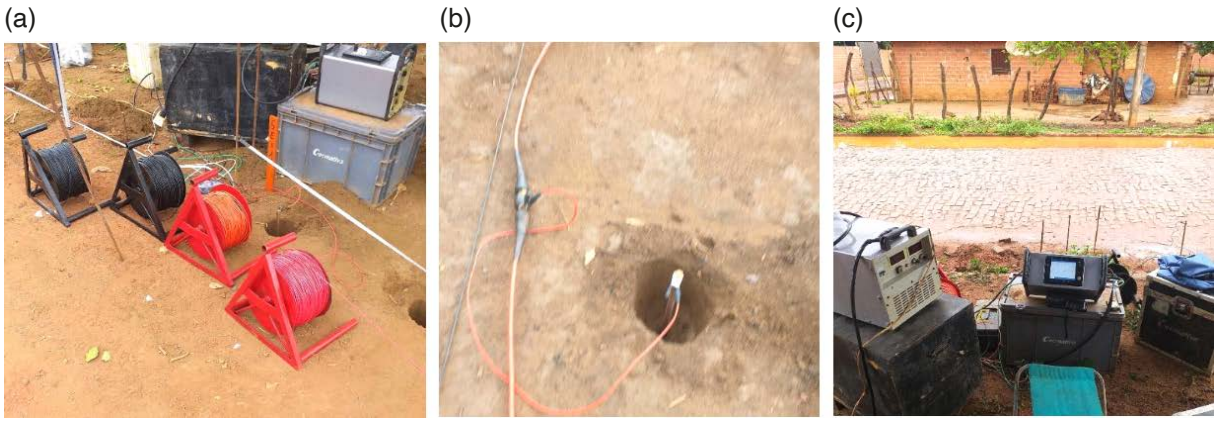

Figure 5. Details of geophysical resistivity survey. Line of IP/resistivity (a), electrode of inoxidizable steel and nonpolarized (b), and GD10 system assembled (c).

This setup ensures precise resistivity measurements and facilitates data interpretation for subsurface investigations. The high injection voltage and current applied, combined with the external power source, enable the survey to penetrate deep subsurface layers, which is essential for identifying aquifers or other geological structures.

During the measurements, several precautions were taken to ensure satisfactory results. The electrodes were aligned and spaced evenly, driven into the ground to a depth of 50 to 80 cm, or until mechanical resistance was encountered. Copper-coated steel electrodes were used, properly cleaned, free of oxidation, and new. The condition of the soil, whether moist or dry, was recorded for control purposes, and the equipment was pre-checked to ensure proper functioning.

To reduce galvanic contact resistance with the soil, salt water was applied around the electrodes. Measurements were taken only on days without the risk of atmospheric discharges, and the team used insulated footwear and gloves as additional safety measures. These careful preparations helped to ensure the accuracy and reliability of the geophysical resistivity data while maintaining a safe working environment.

4.2 Electrical Resistivity method (ERT)

This study was based on the electrical resistivity tomography (ERT) method, utilizing the techniques of Electrical Resistivity Profiling (ERP) and Vertical Electrical Sounding (VES) to measure the subsurface electrical resistivity and determine the stratification of subsurface layers (Telford et al., 1990). This method is grounded in the identification of subsurface geological structures through the electrical properties of materials and serves as a complement to direct investigation methods. The electrical resistance R (Ohms) of a conductor is defined as:

$$R = \frac{\Delta V}{I} \tag{1}$$

where ΔV is the potential difference between two points in the conductor and I is the injected current. It is discovered that the conductor's resistance is inversely related to its cross-sectional area A (m^2) and directly proportional to its length L (m) (Mooney et al., 1966):

$$R = \frac{\rho L}{A} \tag{2}$$

$$\rho = \frac{\Delta V}{I}\frac{A}{L} \tag{3}$$

where the conductor's electrical resistivity is represented by ρ (Ω·m). In an infinite, homogeneous half-space and isotropic medium with a single current source on its surface, the current flows radially away from the source, and the potential varies inversely with distance (r) from the current source. The equipotential surfaces ($2\pi r^2$) have a hemisphere shape, and the current flow is perpendicular to the equipotential surface (Hassan, 2014; Roodposhti et al., 2019). The potential in this case is given by:

$$V = \frac{\rho I}{2\pi r} \tag{4}$$

The measurement of electrical resistivity typically requires four electrodes: two electrodes, referred to as A and B, which are used to inject the current, and two other electrodes, referred to as M and N, which are used to record the resulting potential difference. The potential difference ΔV measured between electrodes M and N is given by the following equation:

$$\Delta V = V_M - V_N = \frac{I\rho}{2\pi}\left(\frac{1}{AM} - \frac{1}{BM}\right) - \left(\frac{1}{AN} - \frac{1}{BN}\right) \tag{5}$$

where AM, BM, NA, and BN represent the geometric distance between electrodes A and M, B and M, A and N, and B and N, respectively. The apparent electrical resistivity ρ_a is then calculated using the following equation:

$$\rho_a = \left[\frac{2\pi}{\frac{1}{AM} - \frac{1}{BM} - \frac{1}{AN} + \frac{1}{BN}}\right]\frac{\Delta V}{I}$$
$$\rho_a = K\frac{\Delta V}{I} \tag{6}$$

where K is the geometric coefficient that depends on the arrangement of the four electrodes A, B, M, and N. The current electrodes (A and B) and the potential electrodes (M and N) can be placed on the ground surface or in boreholes (Fig. 6). Compared to surface methods, cross-borehole methods offer the advantage of higher resolution with depth (Slater and Reeve, 2002).

By utilizing boreholes, the measurements can more accurately capture subsurface resistivity variations, as the electrodes are positioned closer to the geological structures of interest. This allows for a more detailed and reliable stratigraphic interpretation, especially in complex subsurface environments.

Two Electrical Resistivity (ERT) surveys were conducted using Dipole Dipole, Pole Dipole, and Pole Pole configurations, referred to as Line 01 and Line 02 (see Figs. 7 and 11). Additionally, two Vertical Electrical Soundings (VES) were performed using the Schlumberger array, designated as VES 01 and VES 02. These surveys were distributed across Area 1 and Area 2.

For the resistivity profiles (Lines 1 and 2), the Dipole Dipole, Pole Dipole, and Pole Pole configurations were used, reaching investigation depths of 50 m, 60 m, and 200 m, respectively. In all configurations, an electrode spacing of 10 m was maintained. The potential electrodes (MN/2) were spaced at intervals of 25 cm, 1 m, 2.5 m, 10 m, and 25 m, while the current electrodes (AB/2) were spaced at distances of 1.3 m, 1.8 m, 2.4 m, 3.2 m, 4.2 m, 5.5 m, 7.5 m, 10 m, 13 m, 18 m, 24 m, 32 m, 42 m, 55 m, 75 m, 100 m, 130 m, 180 m, 200 m, 300 m, 400 m, and 500 m.

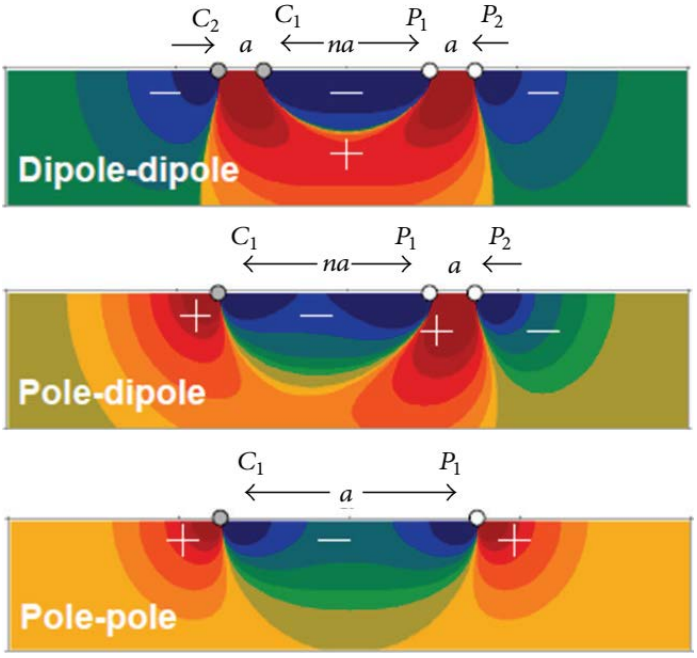

Figure 6. Schematic model of Electrical Resistivity Measurements. (a) Dipole Dipole array, (b) Pole Dipole array, and Pole Pole (modified from Okpoli, 2013).

During the measurements, the system GD10 resistivity meter, used for this project, was equipped with an internal memory capable of storing all measurement data, including resistance (Ohms) and apparent resistivity (Ω·m).

4.3 Inversion of geophysical data

The acquired electrical resistivity pseudosections were interpreted using the inversion method, which aims to find a model whose responses align with the measured data (Loke et al., 2021). To generate the resistivity sections of the inverted model, the software RES2DINV® was employed. The version used in this study was 3.4, "2D Resistivity and IP Inversion," developed by Geotomo Software, Malaysia, and running on the Microsoft Windows® platform (Thibaut et al., 2021).

This software applies the least squares method, where the resistivity values of the model blocks are treated as parameters, while the measured apparent resistivity values serve as input data. It is well known that for a given dataset, multiple models can generate resistivity values that approximate the measured values to varying extents, leading to potential ambiguities (Rocha et al., 2015, 2016; Cardarelli and De Donno, 2019).

In addition to minimizing discrepancies between calculated and measured values, inversion methods also aim to optimize other parameters to produce desirable characteristics in the resulting model. RES2DINV software uses an iterative process with a smoothness constraint, starting from an initial model and progressively refining it to achieve apparent resistivity values that better match the measured data (Boyle and Wilkinson, 2021). The measured apparent resistivity values from the VES were smoothed to reduce the effect of geological noise – lateral variations in geological layers – present in the measurements.

The Vertical Electrical Sounding (VES) data were inverted using the Ridge Regression method through the IX1D® software to obtain more representative subsurface models (Othman et al., 2022). This process allowed the determination of the top and base depths, as well as the thicknesses of the geological units in the study area, along with their respective resistivity's (Da Rocha et al., 2019; ElKaliouby, 2020).

In the interpretation process of the VES data, the thicknesses of the geological units identified in the literature review were used to assist in recognizing these units within the VES curves. This approach facilitated a more precise determination of the (AB/2) spacing that provides the ratio of the geological units' thicknesses, increasing the reliability of the VES interpretative model. A six-layer model was applied to the VES, providing a better fit to the subsurface structure.

Additionally, data from the Groundwater Information System (SIAGAS), developed by the Brazilian Geological Survey (SGB), which provides information on tubular wells across nearly the entire national territory, contributed to the parameterization of the VES in the investigated Areas 1 and 2. This integration supported the development of a more reliable geological model of the subsurface.

5. Results and Discussions

Based on the results obtained from Lines 01 and 02, the Dipole Dipole, Pole Dipole, and Pole Pole configurations revealed evidence of potential groundwater storage structures. These findings suggest the possibility of identifying zones with higher potential for optimal tubular well placement.

Figure 7a shows the location where Line 01 of the geoelectric profile survey was conducted using the Electrical Walk (CE) technique. The black dots indicate the marker stakes, and the blue point represents the location where Vertical Electrical Sounding (VES1) was performed. Figure 7b displays the resistivity pseudosection of the inversion model obtained with the Dipole Dipole array, requiring five iterations to achieve a good fit for the inverted model of the layers down to approximately 50 m depth, with an absolute error of 1.80%. In Fig. 7c, the interpreted geological-geophysical model of the layers can be seen, where four potential groundwater-bearing layers were identified.

Figure 8a presents the resistivity section of the inverse model obtained with the Pole Dipole array, requiring five iterations to achieve a good fit for the inverted model layers, reaching approximately 10 m deeper than the model obtained with the Dipole Dipole array and yielding an absolute error of less than 1%. In Fig. 8b, as in Fig. 7c, the diagram of the interpreted geological-geophysical model of the layers is provided, highlighting the region below Aquifer B.

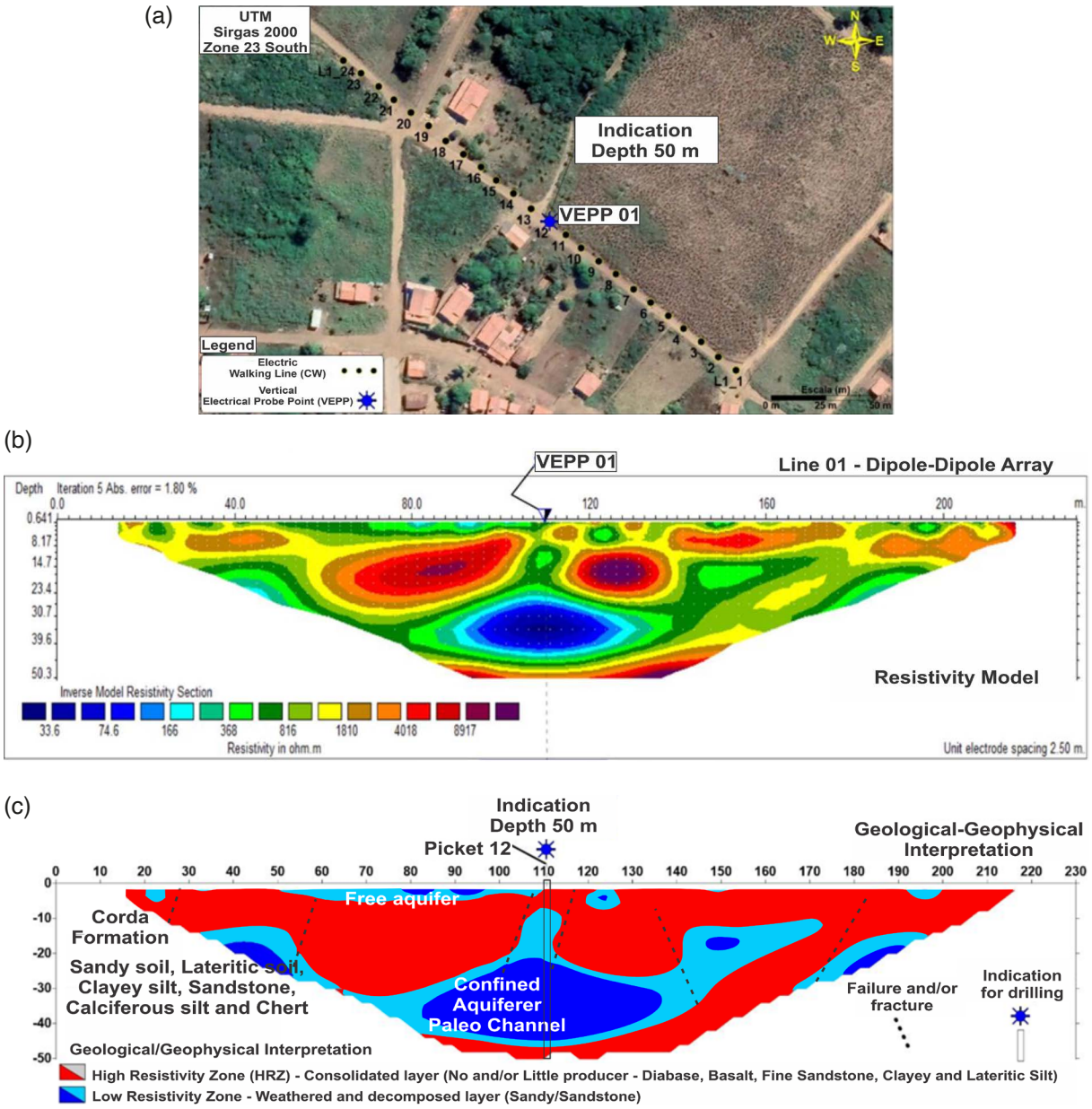

Figure 7. Location map of Area 1 where Line 01 was surveyed (a), resistivity pseudosection of the inversion model based on apparent resistivity measurements with the Dipole Dipole array (b), and diagram of the interpreted geological-geophysical model showing the subsurface at the measurement location (c).

Figure 9a displays the resistivity section of the inverse model obtained with the Pole Pole array. Like Figs. 7b and 8a, five iterations were necessary to achieve a good fit for the inverted layer model, reaching an investigation depth of approximately 170 m with an absolute error around 11.5%. Figure 9b is analogous to Figs. 7c and 8b, illustrating the interpreted geological-geophysical model of the layers, with emphasis on the region beneath Aquifer C, located between the Sardinha and Pastos Bons Formations.

Across the three electrode configurations, a high resistivity zone (HRZ) extending from the start to the end of Line 01 and a low resistivity zone (LRZ) were identified. The HRZ, depicted in red, consists of a consolidated layer composed of diabase, basalt, thin sandstone, silty clay, and lateritic sediments. Conversely, the LRZ is represented in blue and includes weathered and decomposed sediments, primarily sandy/sandstone layers (as seen in Figs. 7c, 8b, and 9b).

Figure 10a presents the resistivity curve for Vertical Electrical Sounding 01 (VES01), demonstrating a strong correlation between the measured and calculated apparent resistivity values. VES01 revealed 13 distinct layers,

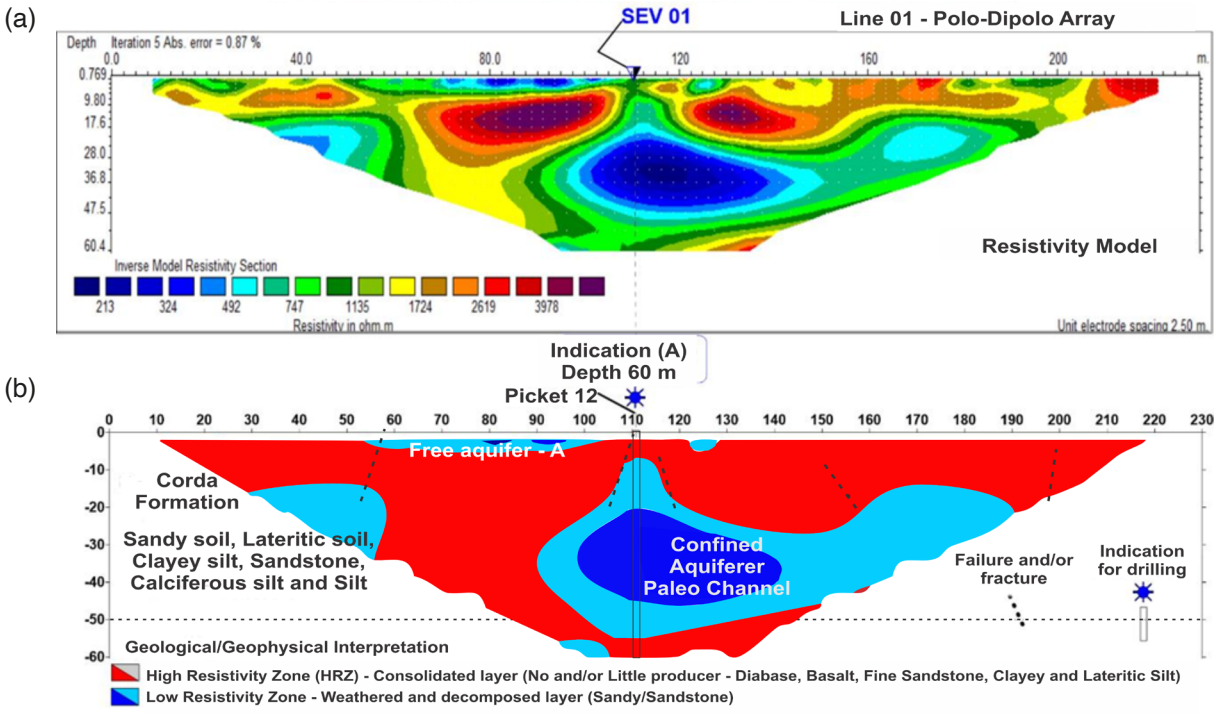

Figure 8. Resistivity pseudosection of the inversion model based on apparent resistivity measurements with the Pole Dipole array (a) and the corresponding interpreted geological-geophysical model diagram, showing the subsurface at the survey location (b).

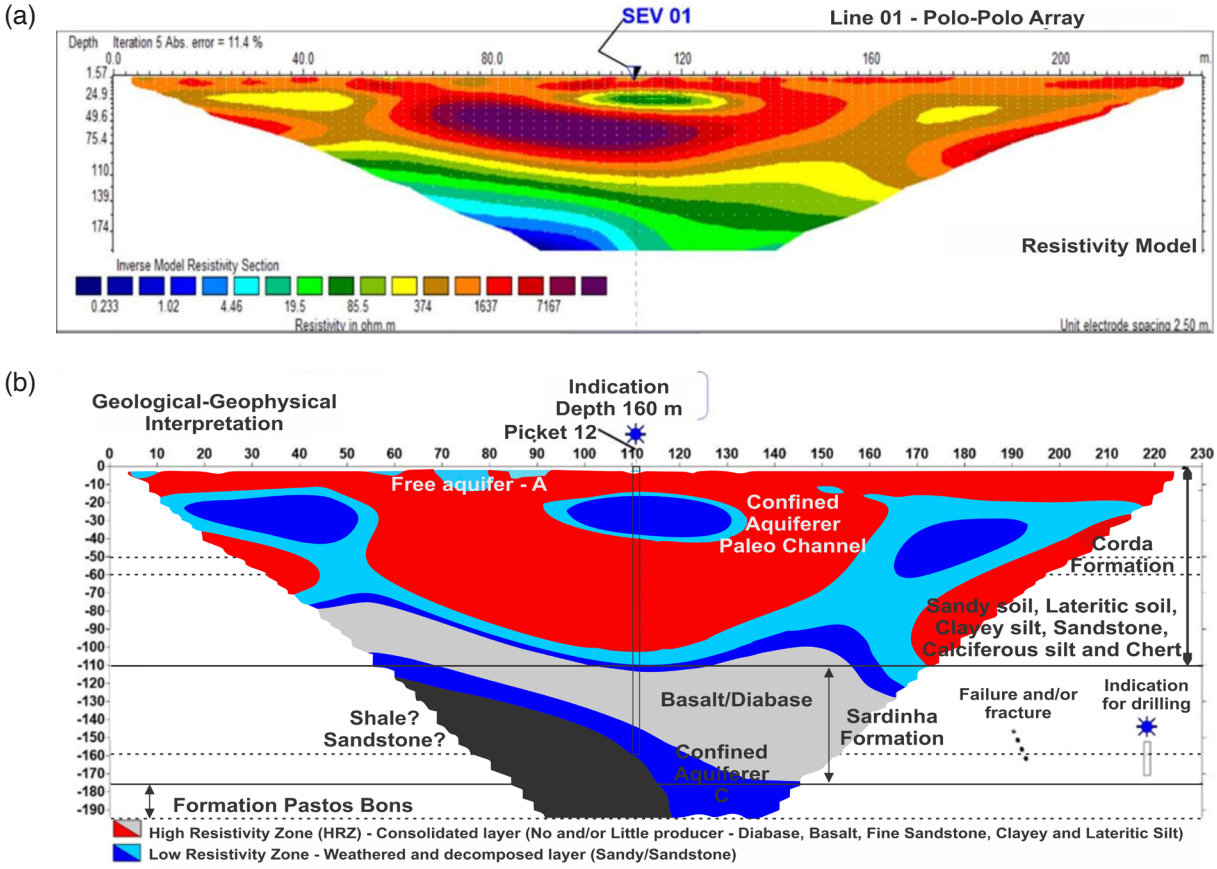

Figure 9. Pseudosection of resistivity for the inversion model based on apparent resistivity measurements with the Pole Pole array (a) and its corresponding interpreted geological-geophysical model diagram showing subsurface layers at the survey site (b).

including four conductive aquifer zones. Figures 10b and 10c offer geological geophysical interpretations along Line 01, highlighting the first layer, identified as a porous, unconfined aquifer (referred to as Aquifer A), extending to a depth of 12 m. However, due to high contamination risk from septic systems, landfills, cemeteries, and other pollution sources, Aquifer A is deemed unsuitable for water supply.

The second layer is interpreted as a confined porous aquifer, characterized as a paleochannel, with its upper boundary at approximately 20 m depth and its base at 50 m. The third aquifer, also confined and referred to as Aquifer B, spans from an upper depth of 100 m to a lower depth of 110 m. The fourth and final aquifer, classified as a confined porous aquifer (Aquifer C), is located between depths of 140 m and 190 m.

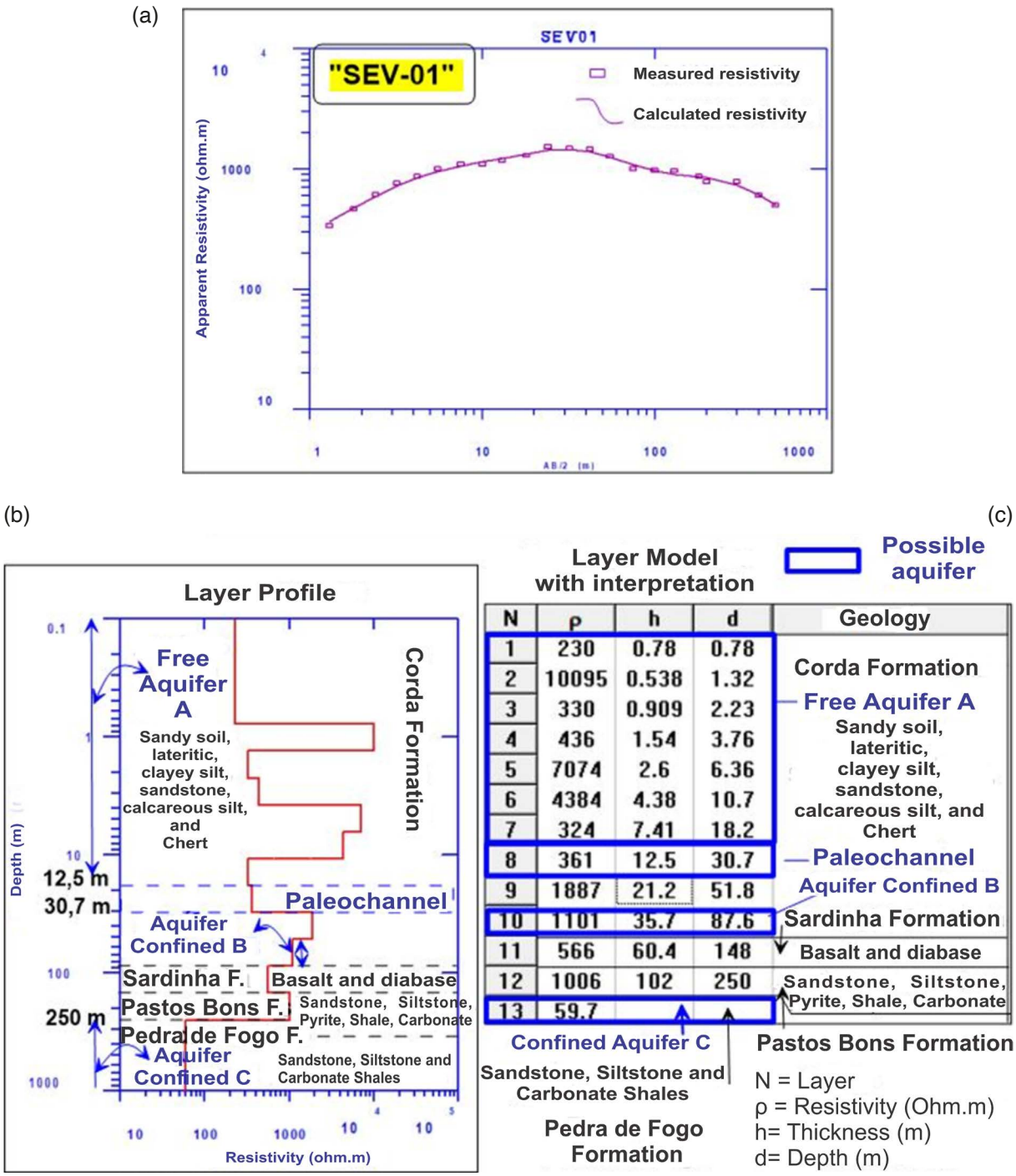

Figure 10. SEV01. (a) Comparison of measured and calculated apparent resistivity values for Vertical Electrical Sounding 01, (b) layer profile illustrating the relationship between resistivity and depth, and (c) interpreted layer model.

Aquifers A and B reflect the geological characteristics of the Corda Formation, which include sandy soils, lateritic materials, silty clay, sandstone, calcareous silt, and chert. Meanwhile, Aquifer C corresponds to the Bons Pastos Formation, characterized by sandstones, pyritic siltstones, schists, and carbonate rocks.

Along Line 01, more resistive zones are observed both near the surface and at greater depths, indicated by green, yellow, orange, red, and purple in the resistivity model sections (Figs. 7b, 8a, and 9a). In contrast, more conductive zones, shown in light to dark blue, suggest the presence of porous aquifers filled with infiltrated water. The resistive zones are interpreted as consolidated layers, comprising weathered and decomposed rock formations.

Figure 11 mirrors the layout of Fig. 7 but illustrates the survey location for Line 02 of the geoelectric profile and the site of Vertical Electrical Sounding (SEV2). Figure 11b shows the resistivity pseudosection of the inversion model using the Dipole Dipole array, where five iterations were required to achieve a satisfactory model fit to approximately 50 m depth, with an absolute error around 13%. Figure 11c presents the interpreted geological-geophysical model of the layers, highlighting the predominance of the high resistivity zone (HRZ).

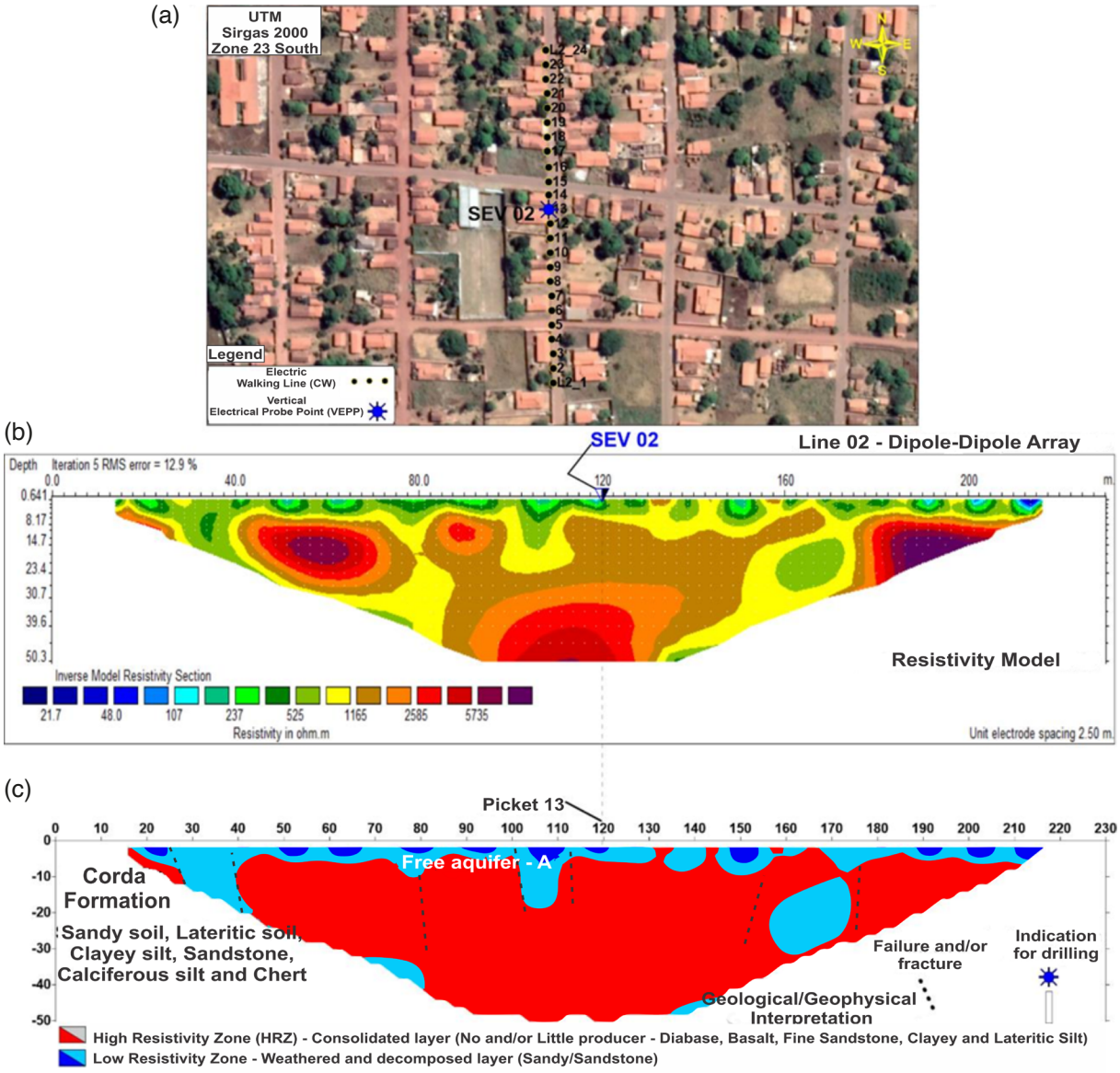

Figure 11. (a) Location map of Area 2 showing the survey conducted along Line 02, (b) resistivity pseudosection of the inversion model based on apparent resistivity measurements using the Dipole Dipole array, and (c) interpreted geological-geophysical model of the subsurface at the measurement site.

Figure 12a resembles Fig. 8a and illustrates the resistivity section of the inverse model along Line 02, obtained using the Pole Dipole array. Here, five iterations were also required to achieve a satisfactory fit of the inverse model, reaching approximately 10 m deeper compared to the Dipole Dipole array model, with an absolute error of less than 5%. In Fig. 12b, only the top of Aquifer B is visible, unlike the interpreted geological-geophysical layer models presented in Fig. 8b.

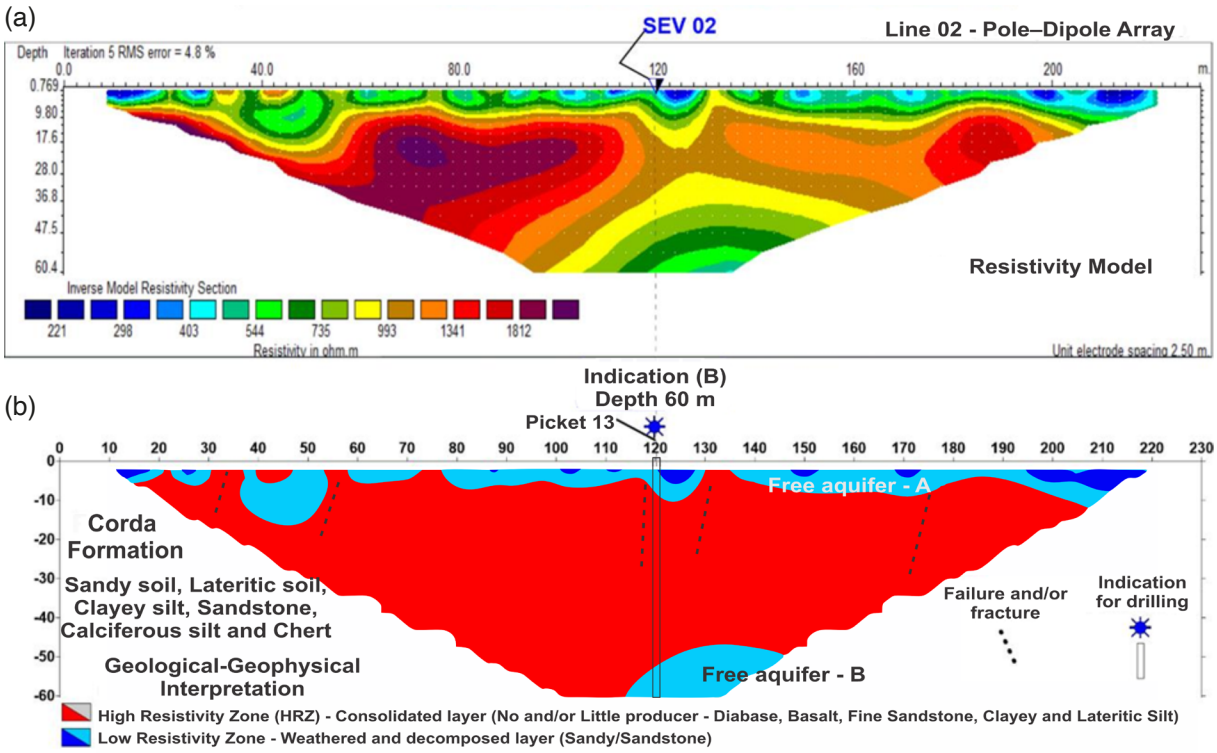

Figure 12. Resistivity pseudosection of the inversion model based on apparent resistivity measurements with the Pole Dipole array (a) and the corresponding interpreted geological-geophysical model diagram, showing the subsurface at the survey location (b).

Figure 13a presents the pseudosection of resistivity from the inversion model, obtained with the Pole Pole array. Like Figs. 11a and 12a, five iterations were required to achieve a satisfactory fit of the inverse model layers, reaching an investigation depth exceeding 200 m with an absolute error of less than 4%. Figure 13b resembles Fig. 9b, displaying a well-defined geological-geophysical model with four layers, highlighting the region below the High Resistivity Zone (HRZ), which includes Aquifer B, the Sardinha Formation marked by basalt/diabase, and the Pastos Bons Formation where confined Aquifer C is located.

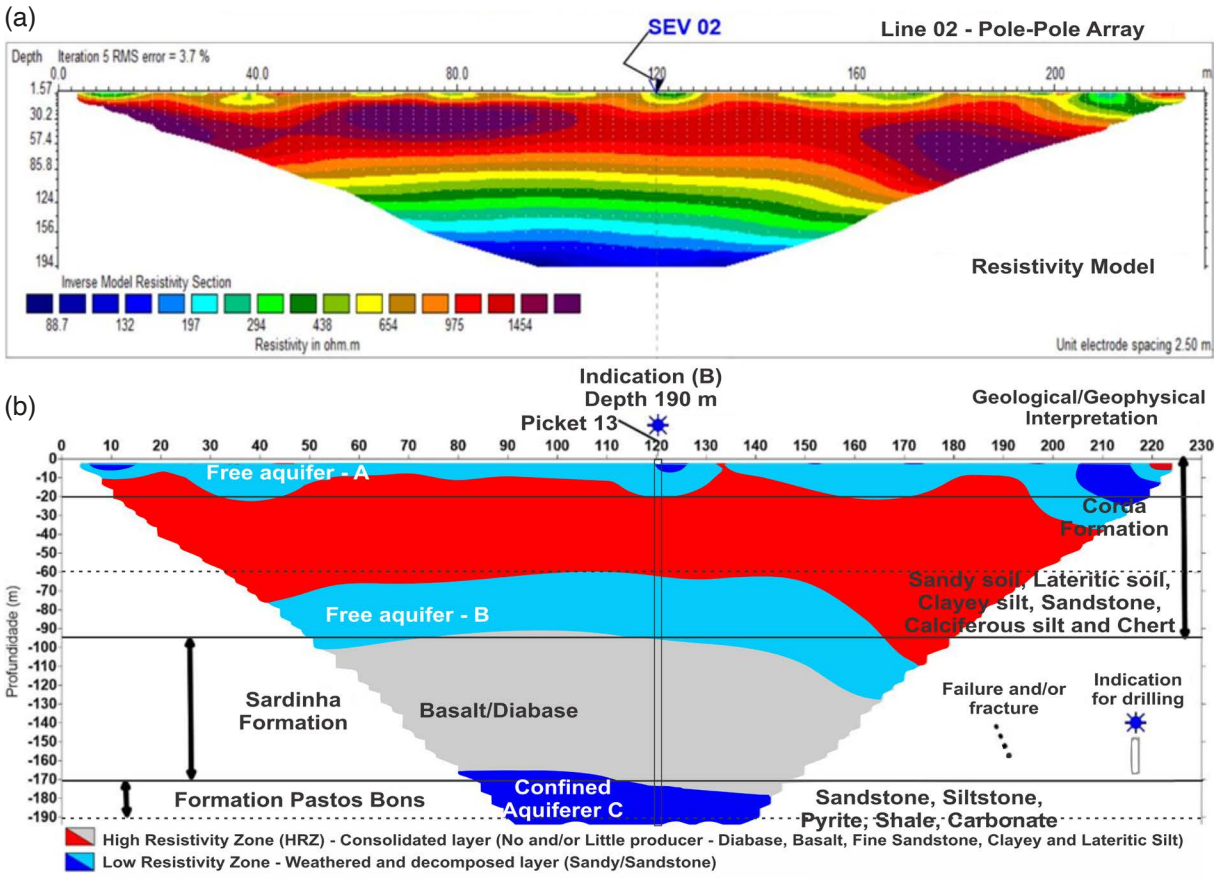

Figure 13. (a) Pseudosection of the resistivity inversion model based on apparent resistivity measurements using the Pole Pole array for Line 02, and (b) its corresponding interpreted geological-geophysical model illustrating the subsurface at the measurement site.

Figure 14 displays the Vertical Electrical Sounding (VES02) and the strong correlation between measured and calculated apparent resistivity values, like VES01, which also identified 13 layers. However, in this case, only three potential groundwater-bearing layers were detected. The first layer, containing Aquifer A – a porous, unconfined aquifer – extends to a depth of 35 m but, as in Line 01, is deemed unsuitable for water supply due to high contamination risk from sources such as septic tanks, landfills, and cemeteries. The second layer is Aquifer B – a porous, confined aquifer – located between depths of approximately 60 m and 90 m. The third layer corresponds to Aquifer C, another porous and confined aquifer, situated between 165 m and 190 m in depth.

The interpretation of the high resistivity layer as a productive aquifer, despite the presence of an underlying layer with lower resistivity, is based on an integration of geophysical and direct geological data, correlated to Fig. 3 and Table 1. Figure 14 confirms the high resistivity layer as a sandstone unit (Pedra de Fogo Formation), whose value is consistent with a well cemented, clean-porous aquifer. The lower resistivity layer is confirmed as massive basalt (Sardinha Formation). While fractured and saturated basalts can exhibit low resistivity, the measured value was interpreted to represent either minimally fractured rock with limited water storage or the conductive signature of clay alteration products, rather than a significant aquifer. This interpretation is further supported by the hydrogeological principle that porous aquifers generally offer more sustainable yields than fractured aquifers in this geological setting.

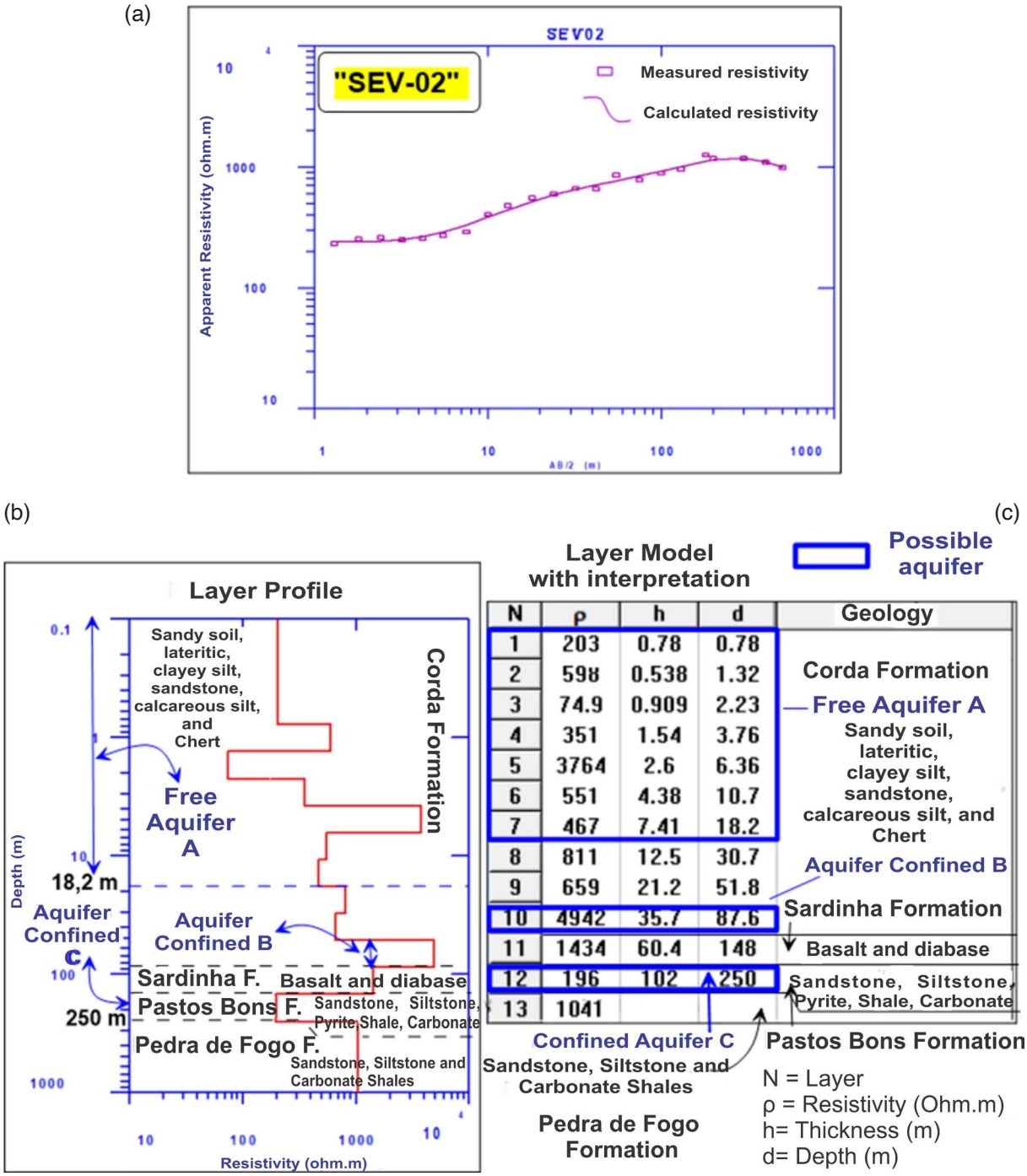

Figure 14. SEV02. Relationship between measured and calculated values from the Vertical Electrical Sounding 02 (a), layer profile illustrating the relationship between resistivity and depth (b), and the interpreted layer model (c).

6. Conclusions

The Electrical Resistivity Tomography (ERT) method provided detailed insights into the subsurface stratigraphy. By measuring variations in the apparent resistivity of geological layers, it was possible to successfully delineate these layers, enabling the identification of aquifer zones and the differentiation of various aquifer types, such as unconfined (Aquifer A) versus confined (Aquifers B and C).

ERT proved effective in mapping lateral variations in apparent resistivity, which was crucial for determining the spatial extent of the aquifers, particularly Aquifers B and C. It facilitated the identification of conductive zones (LRZ), likely corresponding to water-saturated sediments, indicative of promising groundwater reservoirs.

Accurate interpretation of Vertical Electrical Soundings (VES) allowed for precise determination of the thickness and depth of geological units, aiding in the distinction between potentially productive aquifer layers (Sardinha Formation and Pastos Bons Formation) and non-aquifer formations (Corda Formation). This information is essential for locating the optimal drilling depths for wells in Areas 1 and 2, thereby enhancing the likelihood of accessing sufficient groundwater reserves.

The effectiveness of ERT was further enhanced when combined with geological data from existing wells in the SIAGAS database. This integration refined the interpretation of the results from the resistivity pseudosections of the inversion models, with all presenting an absolute error of less than 15%. This improved the reliability of the interpreted geological-geophysical models and the accuracy in predicting aquifer locations and their potential productivity.

Although the ERT method may encounter ambiguities due to complex subsurface structures, the combination of multiple electrode configurations such as Dipole Dipole, Pole Dipole, and Pole Pole arrangements and the use of inversion software like RES2DINV and IX1D helped minimize potential errors and enhance the clarity of the geological-geophysical models.

It is important to emphasize the noninvasive nature of the ERT method, along with its relatively favorable cost-benefit ratio compared to randomly drilling exploration wells without prior study. This positions ERT as a highly suitable investigation tool for groundwater exploration, significantly reducing the risks and costs associated with unproductive drilling. It is recommended that relevant authorities raise public awareness about the importance of adopting sanitary protection measures, particularly regarding the surface layers (Aquifer A) to mitigate risks of groundwater contamination by pollutants. Annual physicochemical analyses of the wells should also be conducted.

Finally, based on the interpreted geological-geophysical models, it is recommended to drill and allocate two tubular wells for groundwater extraction from Aquifer C to mitigate the effects of potable water scarcity during prolonged droughts caused by extreme events associated with climate change. The first well, with a minimum depth of 160 m, should be in Area 1 at station 12 of Line 1. The second well, with a minimum depth of 270 m, should be situated in Area 2 at station 13 of Line 2.

Data availability statement. The datasets generated and analyzed during the current study are available from the corresponding author upon reasonable request.

Acknowledgements. The authors express their gratitude to the Geological Survey of Brazil (CPRM) and the Groundwater Information System (SIAGAS) for providing access to essential data that supported this study. We are also thankful to GeoProspecto Solutions in Geophysics Company Inc (GEOPROSPECTO) for the available equipment used in this research and assistance for teams in the geophysical and hydrogeological surveys, as well as providing logistical support. Special thanks go to the UFRJ and UFRA for their continuous encouragement and infrastructure support for the dataset processing.

References

Ab'Saber, A. N. (1960). Contribuição à geomorfologia do Estado do Maranhão, Not. Geomorfol., 3, 5, 35-45.

Aguiar, A. L., M. MartaAlmeida, M. Cirano, J. Pereira et al. (2024). Numerical assessment of tidal potential energy in the Brazilian Equatorial Shelf, Renew. Energ., 220, 119684, doi:10.1016/j.renene.2023.119684.

Barreto, H. N., M. E. Dantas, E. D. Pereira and J. H. S. dos Santos (2024). Geomorphology of Maranhão State, in Geomorphology of the Northeast Region of Brazil, Springer, Cham, 17-48.

Barreto, H. N., C. K. Parise and E. B. de Almeida (2019). The cocais forest landscape, in The Physical Geography of Brazil: Environment, Vegetation and Landscape, Springer, Cham, 151-167, doi:10.1007/978-3-030-04333-9_8.

Bastos, R. C., L. S. Brasil, F. G. Carvalho, L. B. Calvão et al. (2019). Odonata of the state of Maranhão, Brazil: Wallacean shortfall and priority areas for faunistic inventories, Biota Neotrop., 19, 4, e20190734, doi:10.1590/1676-0611-bn-2019-0734.

Boyle, A. and P. Wilkinson (2021). Geophysical ERT, in Electrical Impedance Tomography, CRC Press, 383-402.

Brito Neves, B. B. D. (1998). The CambroOrdoviciano of the Borborema Province, Bol. IGUSP, Sér. Cient., 29, 175-193.

Brito, P. M. and V. Gallo (2002). A new pleuropholid, Gondwanapleuropholis longimaxillaris ng, n. sp. (Actinopterygii: Teleostei) from the Jurassic of northeast Brazil, C. R. Palevol, 1, 8, 697-703, doi:10.1016/S1631-0683(02)00080-5.

Cardarelli, E. and G. De Donno (2019). Advances in electric resistivity tomography: Theory and case studies, in Innovation in nearsurface geophysics, Elsevier, 23-57, doi:10.1016/B978-0-12-812429-1.00002-7.

Castany, G. (1982). Principes et méthodes de l´hydrogéologie, Bordas Editions, 236.

Correa-Martins, F. J. (2019). The Neostratotype of Itapecuru Formation (LowerMiddle Albian) and Its Impact for Mesozoic Stratigraphy of Parnaíba Basin, An. Acad. Bras. Cienc., 91, Suppl. 2, e20180730, doi:10.1590/0001-3765201920180730.

Correia Filho, F. L., É. R. Gomes, O. O. Nunes and J. B. Lopes Filho (2011). Projeto cadastro de fontes de abastecimento por água subterrânea: estado do Maranhão: relatório diagnóstico do município de Carolina, CPRM.

Da Rocha, H. O., J. A. dos Reis Júnior, P. Andrés, C. Oliva et al. (2019). Detection of aquifer zones by integration geophysical methods HLEM and VES in the Southeast region of Pará, Brazil, OSR J. Appl. Geol. Geophys., 7, 6, 114, doi:10.9790/0990-0706010114.

Da Silva, P. H. M., E. F. J. de Sá, Z. S. de Souza and V. C. Córdoba (2020). Structural controls and stratigraphic setting of sills: Example of the Central Atlantic Magmatic Province in the Parnaíba Basin, Northeast Brazil, J. S. Am. Earth Sci., 101, 102606, doi:10.1016/j.jsames.2020.102606.

Dantas, J. S., J. Marques Júnior, M. V. Martins Filho, J. M. D. A. Resende et al. (2014). Gênese de solos coesos do leste maranhense: relação solopaisagem, Rev. Bras. Cienc. Solo, 38, 1039-1050, doi:10.1590/S0100-06832014000400001.

De Castro, D. L., D. C. Oliveira and M. H. B. Hollanda (2018). Geostatistical interplay between geophysical and geochemical data: mapping lithostructural assemblages of Mesozoic igneous activities in the Parnaíba Basin (NE Brazil), Surv. Geophys., 39, 683-713, doi:10.1007/s10712-018-9463-5.

Dos Reis, L. C., C. M. S. E. Silva, B. G. Bezerra, P. R. Mutti et al. (2020). Analysis of climate extreme indices in the MATOPIBA region, Brazil, Pure Appl. Geophys., 177, 4457-4478, doi:10.1007/s00024-020-02474-4.

ElKaliouby, H. (2020). Mapping sea water intrusion in coastal area using timedomain electromagnetic method with different loop dimensions, J. Appl. Geophys., 175, 103963, doi:10.1016/j.jappgeo.2020.103963.

Feitosa, A. C. (2006). Relevo do Estado do Maranhão: uma nova proposta de classificação topomorfológica, in Simpósio Nacional de Geomorfologia, Regional Conference on Geomorphology, 6, 1-11.

Feitosa, A. C. and J. R. Trovão (2006). Atlas escolar do Maranhão: espaço geohistórico e cultural, Grafset, 207, ISBN:8587872354.

Feitosa, A. C., D. C. Rufino, E. C. Pedrosa, I. da Rocha Barboza et al. (2024). Indicadores socioambientais do clima semiárido no leste maranhense, Rev. Territorium Terram, 7, 12, 414-430, ISSN:2317-5419.

Freeze, R. A. and J. A. Cherry (1979). Groundwater, PrenticeHall, Englewood Cliffs, New Jersey, 604, ISBN:0-13-365312-9.

Góes, A. M. and F. J. Feijó (1994). Parnaiba Basin; Bacia do Parnaiba, Bol. Geocienc. Petrobras, 8, 1, 103-109.

Hassan, A. (2014). Electrical resistivity method for water content characterisation of unsaturated clay soil, Doctoral dissertation, Durham University.

Hiscock, K. M. and V. F. Bense (2014). Hydrogeology: principles and practice, John Wiley & Sons, 544, ISBN:9780470656631.

Klein, A. H. D. F. and A. D. Short (2023). Physical Characteristics of Brazilian Sandy Beaches, in Brazilian Sandy Beaches, Springer, Cham, 130, doi:10.1007/978-3-031-30746-1_1.

Loke, M. H., D. F. Rucker, J. E. Chambers, P. B. Wilkinson et al. (2021). Electrical resistivity surveys and data interpretation, in Encyclopedia of Solid Earth Geophysics, Springer, Cham, 344-350, doi:10.1007/978-90-481-8702-7_46.

Maranhão (2002). Atlas of Maranhão, Labogeo, São Luís.

Mendes, M. S. (2007). Stratigraphic analysis of the Grajaú-Codó formational interval (Aptian) in the Parnaíba Basin, NE Brazil, M.Sc. Dissertation, Federal University of Rio de Janeiro.

Mendes, M. F., J. G. D. V. Alves and M. W. C. Silva (2014). Prospecção geofísica para delimitação do contato das formações Itapecuru e Codó no município de Jacundá PA, Aguas Subterr., 28, 1, doi:10.14295/ras.v28i1.27401.

Mooney, H. M., E. Orellana, H. Pickett and L. Tornheim (1966). A resistivity computation method for layered earth models, Geophysics, 31, 1, 192-203, doi:10.1190/1.1439733.

Okpoli, C. C. (2013). Sensitivity and resolution capacity of electrode configurations, Int. J. Geophys., 2013, 1, 608037, doi:10.1155/2013/608037.

Oliveira, A. L., M. M. Pimentel, R. A. Fuck and D. C. Oliveira (2018). Petrology of Jurassic and Cretaceous basaltic formations from the Parnaíba Basin, NE Brazil: correlations and associations with large igneous provinces, Geol. Soc. Lond. Spec. Publ., 472, 1, 279-308, doi:10.1144/sp472.21.

Othman, A. A., A. M. Beshr, A. M. Abd ElGawad and I. M. Ibraheem (2022). Hydrogeophysical investigation using remote sensing and geoelectrical data in southeast Hiw, Qena, Egypt, Geocarto Int., 37, 26, 14241-14260, doi:10.1080/10106049.2022.2087750.

Pereira, P. B., H. K. de Brito Nunes and A. da Silva Sousa (2022). Caracterização geoambiental do município de Caxias, Maranhão/Brasil, Geogr. Atos, 6, 119, doi:10.35416/geoatos.2022.8897.

Reimold, W. U., L. Ferrière, Á. P. Crósta, M. A. R. Vasconcelos et al. (2022). Nova Colinas, Maranhão State: A newly confirmed, complex impact structure in Brazil, Meteorit. Planet. Sci., 57, 8, 1519-1541, doi:10.1111/maps.13833.

Rocha, H., M. W. C. Silva, F. L. T. Marques and D. C. Leite Filho (2015). Magnetic gradiometry and ground penetrating radarapplied in Estearia of Penalva (MA), Geol. USP, Ser. Cient., 15, 1, 314, doi:10.11606/issn.2316-9095.v15i1p3-14.

Rocha, H., L. Costa and J. Júnior (2016). Geotechnical investigation using SP, Electroresistivity and GPR geophysical methods, Geotecnia, 137, 141-155, doi:10.24849/j.geot.2016.137.09.

Rodrigues, R. (1995). Organic geochemistry of the Parnaíba Basin, Ph.D. Thesis, Federal University of Rio Grande do Sul, UFRGS.

Roodposhti, H. R., M. K. Hafizi, M. R. S. Kermani and M. R. G. Nik (2019). Electrical resistivity method for water content and compaction evaluation, a laboratory test on construction material, J. Appl. Geophys., 168, 49-58, doi:10.1016/j.jappgeo.2019.05.015.

Rossetti, D. F., J. D. Paz and A. M. Góes (2004). Facies analysis of the Codó formation (late Aptian) in the Grajaú area, southern São LuísGrajaú Basin, An. Acad. Bras. Cienc., 76, 791-806, doi:10.1590/S0001-37652004000400012.

Rossi, J. B., A. S. Fleischmann, L. Laipelt, B. C. de Andrade et al. (2024). How much evaporation occurs in Brazilian reservoirs? A multimodel perspective, J. S. Am. Earth Sci., 140, 104899, doi:10.1016/j.jsames.2024.104899.

Sandberg, S. K., L. D. Slater and R. Versteeg (2002). An integrated geophysical investigation of the hydrogeology of an anisotropic unconfined aquifer, J. Hydrol., 267, 34, 227-243, doi:10.1016/S0022-1694(02)00153-1.

Schwartz, F. W. and H. Zhang (2024). Fundamentals of groundwater, John Wiley & Sons, 512, ISBN:978-1-119-82013-0.

Silva, F. B., J. R. N. Santos, F. E. C. S. Feitosa, I. D. C. Silva et al. (2016). Evidências de mudanças climáticas na região de transição AmazôniaCerrado no Estado do Maranhão, Rev. Bras. Meteorol., 31, 3, 330-336, doi:10.1590/0102-778631320150149.

Silva-Moraes, H. G., I. Cordeiro and N. Figueiredo (2019). Flora and floristic affinities of the Cerrados of Maranhão State, Brazil, Edinb. J. Bot., 76, 1, 121, doi:10.1017/S0960428618000215.

Slater, L. D. and A. Reeve (2002). Investigating peatland stratigraphy and hydrogeology using integrated electrical geophysics, Geophysics, 67, 2, 365-378, doi:10.1190/1.1468597.

Sophocleous, M. (2002). Interactions between groundwater and surface water: the state of the science, Hydrogeol. J., 10, 52-67, doi:10.1007/s10040-001-0170-8.

Telford, W. M., L. P. Geldart and R. E. Sheriff (1990). Applied Geophysics, Cambridge University Press, 792, doi:10.1017/CBO9781139167932.

Thibaut, R., T. Kremer, A. Royen, B. K. Ngun et al. (2021). A new workflow to incorporate prior information in minimum gradient support (MGS) inversion of electrical resistivity and induced polarization data, J. Appl. Geophys., 187, 104286, doi:10.1016/j.jappgeo.2021.104286.

Vaz, P. T., J. R. Wanderley Filho and W. A. S. Travassos (2007). Bacia do Parnaíba, Bol. Geocienc. Petrobras, 15, 2, 253-263.

Veras, D. S., E. R. Castro, G. S. Lustosa, C. A. S. de Azevêdo et al. (2019). Evaluating the habitat integrity index as a potential surrogate for monitoring the water quality of streams in the cerradocaatinga ecotone in northern Brazil, Environ. Monit. Assess., 191, 19, doi:10.1007/s10661-019-7667-x.

Zanin, P. R., R. B. L. Cavalcante, A. S. Fleischmann, C. A. Peres et al. (2024). Do protected areas enhance surface water quality across the Brazilian Amazon?, J. Nat. Conserv., 81, 126684, doi:10.1016/j.jnc.2024.126684.

Appendix A.

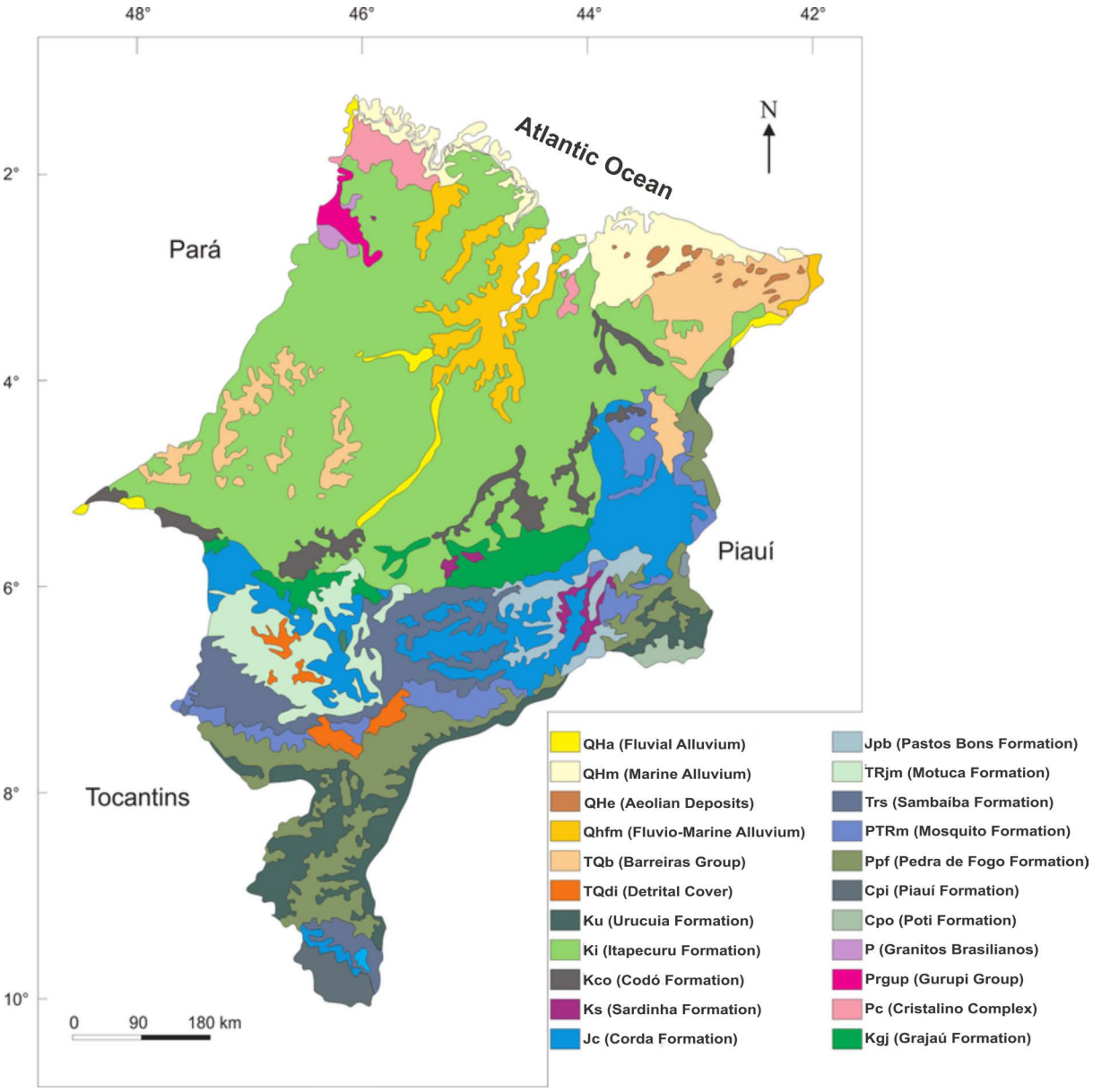

Figure A1. Geological map of the Maranhão state in Brazil (modified from Maranhão, 2002 and Rocha et al., 2015).

***CORRESPONDING AUTHOR: Herson ROCHA**,
Federal University of Rio de Janeiro (UFRJ), Polytechnical Institute (IPOLI), Rio de Janeiro, Brazil
email: herson.rocha@macae.ufrj.br